Strong influence of the entrance channel on the formation of compound nuclei ^{216,222}Th* and their evaporation residues

G. Fazio, G. Giardina,* G. Mandaglio, and R. Ruggeri
INFN, Sezione di Catania, and Dipartimento di Fisica dell'Università di Messina, 98166 Messina, Italy

A. I. Muminov
Heavy Ion Physics Department, Institute of Nuclear Physics, 702132 Tashkent, Uzbekistan

A. K. Nasirov,† Yu. Ts. Oganessian, A. G. Popeko, R. N. Sagaidak, and A. V. Yeremin
Flerov Laboratory of Nuclear Reactions, JINR, 141980 Dubna, Russia

S. Hofmann
Gesellschaft für Schwerionenforschung mbH, 64291 Darmstadt, Germany

F. Hanappe
Université Libre de Bruxelles, 1050 Bruxelles, Belgium

C. Stodel
GANIL, 14076 Caen, France

(Received 20 June 2005; published 22 December 2005)

The dynamical effects of the entrance channel on the formation of the evaporation residues are studied by analyzing the ^{40}Ar + ^{176}Hf, ^{86}Kr + ^{130,136}Xe, ^{124}Sn + ^{92}Zr, and ^{48}Ca + ^{174}Yb reactions leading to the ^{216}Th* and ^{222}Th* compound nuclei. We find that the difference between the evaporation residue cross sections for the reactions leading to the same compound nucleus is caused by the different angular momentum distributions of the partial fusion cross sections $\sigma_{\rm fus}^{\ell}(E_{\rm c.m.})$. The strong dependence of the fusion angular momentum distribution on the mass (charge) asymmetry and shell structure of reactants is demonstrated. The effect of the A/Z ratio for the ^{86}Kr + ^{130,136}Xe reactions is discussed. The dynamical conditions of capture affect the competition between complete fusion and quasifission and, consequently, the shape of the angular momentum distribution of the compound nucleus. By this way the peculiarities of the entrance channel also affect the fission-evaporation competition of the excited intermediate nuclei along the deexcitation cascade of the compound nucleus and, consequently, the evaporation residue formation.

DOI: 10.1103/PhysRevC.72.064614 PACS number(s): 25.70.Jj, 25.70.Gh, 25.70.Lm, 25.85.Ge

I. INTRODUCTION

The study of the role of the entrance channel in the formation of evaporation residues is an actual problem in establishing the optimal conditions for the synthesis of new superheavy elements. Comparison of the excitation functions of evaporation residues (ER) measured for different mass asymmetry reactions but leading to the same compound nucleus (CN) allows us to analyze the importance of the entrance channel effects on the fusion-fission reaction mechanism in collisions of massive nuclei. Often excitation functions of evaporation residues, measured in various reactions leading to the same compound nucleus, are different not only in the position of the maximum but also in the value of their maximums. The analysis of the experimental data of different fusion-fission reactions leading to the same CN allows us to reach useful conclusions about the mechanism of the fusion-fission process.

The analysis of data obtained from experiments in GSI (Darmstadt) and Flerov Laboratory of Nuclear Reactions (Dubna) reveals that the maximum value of the ER cross sections $\sigma_{ER}(E_{\rm c.m.})$ for ^{40}Ar + ^{176}Hf [1,2] is about 12 times larger than for ^{86}Kr + ^{130}Xe [3] and 3 times larger than for ^{124}Sn + ^{92}Zr [4]. All of these reactions lead to the same excited ^{216}Th* compound nucleus. The ^{40}Ar + ^{176}Hf reaction has a larger mass asymmetry [$\eta_A = |A_2 - A_1|/(A_1 + A_2)$] in comparison with the other two. But an intriguing phenomenon is that the measured maximum value of $\sigma_{ER}(E_{\rm c.m.})$ for the ^{124}Sn + ^{92}Zr reaction is about 4 times larger than that for the ^{86}Kr + ^{130}Xe reaction, nearly at the same E^* value, though the mass asymmetry of the ^{124}Sn + ^{92}Zr reaction ($|\eta_A| = 0.148$) is smaller than the one of the ^{86}Kr + ^{130}Xe reaction ($|\eta_A| = 0.204$).

But, in the case of the ^{48}Ca + ^{174}Yb and [5] ^{86}Kr + ^{136}Xe [3] reactions leading to the excited ^{222}Th* compound nucleus, the comparison of the measured data on the cross sections of evaporation residues does not show strongly the role of the mass asymmetry of the entrance channel.

The influence of the neutron number (or the A/Z ratio) of reactants on the measured ER was studied by comparing the

*Electronic address: giardina@nucleo.unime.it
†Also at Heavy Ion Physics Department, INP, Tashkent, Uzbekistan.

results of the reactions with the ^{86}Kr beam on the ^{130}Xe and ^{136}Xe targets. The difference between the experimental data on ERs in the above-mentioned reactions shows a connection with their dependence on the fusion angular momentum distribution, which is determined by the peculiarities of the potential energy surface calculated as a function of the relative distance between centers of nuclei and mass (charge) asymmetry. It should be stressed that the potential energy surface depends on such characteristics of the entrance channel as the shell structure [6–8] and orientation angles of the axial symmetry axis of colliding nuclei relative to the beam [9].

The aim of this article is to interpret the difference between the experimental data for the ^{40}Ar + ^{176}Hf [1,2], ^{86}Kr + ^{130}Xe [3], and ^{124}Sn + ^{92}Zr [4] reactions leading to the ^{216}Th* compound nucleus and the ^{48}Ca + ^{174}Yb [5] and ^{86}Kr + ^{136}Xe [3] reactions leading to the ^{222}Th* compound nucleus by analyzing the role of the mass asymmetry and shell structure of the projectile and target nuclei. In this article, we compare the calculated excitation functions of the complete fusion, quasifission, and fast-fission with the measured fission excitation function for the ^{40}Ar + ^{176}Hf reaction. The experimental data were obtained from the detection of the reaction products of symmetric masses. Note those products could be formed not only at the fission of the hot CN but also at quasifission of DNS, which lives long enough to reach mass equilibration in the subsequent reseparation process.

The models based on the dinuclear system (DNS) concept [6–8,10–12] allows one to estimate both contributions of the fusion-fission and quasifission processes for a massive system or for a symmetric entrance channel in the case of midheavy systems. The strong decrease of the fusion probability is caused by the increase of the quasifission events when the charge numbers of projectile (Z_1) and target (Z_2) lead to $Z_1Z_2 > 1600$. The competition between complete fusion and quasifission is not monotonic function, decreasing by increasing Z_1Z_2. Although $Z_1Z_2 = 2000$ for the ^{124}Sn + ^{92}Zr reaction, the rate of the quasifission events seems to be smaller than that for the ^{86}Kr + ^{130}Xe reaction, which is $Z_1Z_2 = 1944$. We show that it is connected with the influence of peculiarities of the shell structure in reactants on the competition between complete fusion and quasifission processes.

The transformation of the DNS formed at the capture process into compound nucleus is hindered because of the competition of the complete fusion with the quasifission process. The latter means a decay of DNS before reaching the compound nucleus state during its evolution.

If the reacting nuclei in the entrance channel are not massive and have enough energy to overcome the Coulomb barrier, the complete fusion cross section is comparable with the capture cross section. The reaction mechanism is not complicated and the fusion cross section can be described in the framework of the well-known models [13,14]. In this case, a real presentation of the reaction mechanism leading to the complete fusion can be obtained from the characteristics of the detected reaction products. The deexcitation cascade of the heated compound nucleus can be correctly and easily analyzed as a competition between fission and evaporation processes in the framework of the standard statistical model, which takes into account the dependence of the damping of shell corrections to the fission barrier by increasing of the excitation energy. Moreover, it is possible to estimate the influence and evolution of these effects at changing of the beam energy and orbital angular momentum.

Such characteristics of reactions as the mass, charge, and kinetic energy distributions with the related variances of the fission and quasifission fragment distributions, as well as the asymmetry of their angular distributions at different energies can give important information on the reaction mechanism. The analysis of those characteristics of the reaction to study the fusion mechanism becomes a complicated procedure when other processes such as quasifission and fast-fission can compete with the complete fusion in the entrance channel.

The complexity of the estimation of the true fusion cross sections for reactions with massive nuclei is connected with the identification of the fusion-fission fragments among other fissionlike fragments as quasifission, fast-fission fragments, and deep-inelastic collisions at which the evolution of the dinuclear system does not reach the equilibrated compact shape of a compound nucleus. Quasifission and fast-fission reactions are binary processes leading to the formation of products that have the characteristics similar to the fusion-fission fragments, as the full relaxation of the relative kinetic energy and a considerable transfer of mass between the two constituents of DNS. We should state that the quasifission can occur at the all values of the orbital angular momentum, whereas the fast-fission occurs only at high values of the orbital angular momentum.

In experiments in Refs. [15–20], where binary reaction products were studied, the fusion-fission cross sections are derived from counting of the mass symmetric fission events. But an important question is whether all the mass symmetric fission fragments originate from compound nuclei. Is there a possibility splitting the fully equilibrate composite system (mononucleus) under the strong Coulomb repulsion into two symmetric fragments without forming a compound nucleus? This question is connected with correct understanding of the fusion mechanism of massive nuclei. In reactions with massive nuclei, the measured value of the evaporation residue cross section is some microbarn or lower, whereas the estimated value of the fusion cross section, using some assumptions, is several hundreds millibarn. Because of the small fission barrier and large excitation energy of the formed compound nucleus, the fission products give the main contribution to the measured data. Consequently, the fission cross section is equal to the fusion cross section. This conclusion is not correct if the fissionlike products are mixed with the those of the quasifission and fast-fission processes. The decay of DNS after relaxation of the mass asymmetry degree of freedom without formation of compound nucleus is called quasifission. Fast-fission is a binary process that occurs only at high values of the orbital angular momentum. It is a disintegration into two fragments of the mononucleus that has very high angular momentum and survives against quasifission. Moreover, it is well known that the fission barrier for a compound

nucleus decreases by increasing of its angular momentum and disappears at the definite value ℓ_f [21]. Because of the contribution of a large number of orbital angular momenta (or impact parameters), the complete fusion could occur at the large values of the angular momentum [22,23]. Therefore, the mononucleus, having high a angular momentum, splits into two fragments immediately if its angular momentum is larger than ℓ_f, because there is no barrier providing stability. Products of this splitting have alike characteristics as that of the usual fission of the compound nucleus and they can be separated only by the detailed measurements of their angular distributions. It was found in Ref. [24] that, in reactions with massive nuclei used to synthesize superheavy elements, 90–99% of mass symmetric fission events come from the quasifission in which the system does not reach the spherical compact shape. Therefore, it is necessary to estimate how much part of the mass symmetric events belongs to the genuine fusion-fission process going through the formation of the compound nucleus with a compact shape. Moreover, there is not an unambiguous conclusion about the fusion mechanism of massive nuclei though investigators found good agreement with the systematics of the experimental data on the evaporation residues or/and yields of the mass symmetric fragments ($M_1 + M_2 \approx M_{\text{projectile}} + M_{\text{target}}$). Because the used assumptions in the analysis of the experimental data lead to conflicting conclusions about the fusion mechanism [4,25–33].

Another intriguing task is a plausible explanation of the difference between the evaporation residue cross sections for two different reactions leading to the "same" compound nucleus at the same excited energy, and to draw reasonable conclusions, if we could know the fusion cross section and the fusion angular momentum distribution (partial fusion cross section). The last one is not the same for two reactions with different charge asymmetry because of the different rates of the competition between the complete fusion and quasifission processes on $E_{\text{c.m.}}$ and ℓ the entrance channel. Consequently, the fission-evaporation competition during the deexcitation cascade of the "same" compound nuclei having different angular momentum distributions will be different because of the dependence of the fission barrier and α-particle emission probability on the angular momentum. So, it is clear now that two reactions with different mass asymmetries in the entrance channel lead to different values and shapes of the fusion excitation functions [32]. The compound nuclei with different angular momentum distributions cannot be considered the "same" CN even if they have the same excitation energy. Consequently, those compound nuclei formed by different reactions have not the same decay peculiarities.

Therefore, the evaporation residue yields are affected by the dynamics of the entrance channel and by the different fission probability of the "same" excited compound nucleus obtained by different combinations of massive reacting nuclei. Note the nucleus-nucleus potential, moment of inertia and intrinsic fusion barrier depend on the mass asymmetry, shape and shell structure of the reactants.

The study of the evolution of the dinuclear system can show the origination of the reaction products, whether they are the quasifission products [24,34,35] or the fusion-fission products. Our method of calculation (also including the advanced statistical method [36–38]) of the evaporation residue cross sections takes into account the damping of the shell correction in the fission barrier as a function of the nuclear temperature and orbital angular momentum. This is accounted for the various steps of the deexcitation cascade of the compound nucleus leading to the fission fragments or the evaporation residue nuclei in the exit channel [22,23,32,39].

The structure of the article is as follows. The main peculiarities of capture and complete fusion in competition with quasifission and fast-fission processes are described in Sec. II. In Sec. III, we compare the results of calculation with the experimental data for the reactions leading to the ^{216}Th* and ^{222}Th* compound nuclei, and we discuss the effect of the entrance channel on the reaction mechanism. Conclusions are presented in Sec. IV.

II. ABOUT PECULIARITIES OF CAPTURE AND COMPLETE FUSION IN COMPETITION WITH QUASIFISSION AND FAST-FISSION

The capture cross section at given beam energy $E_{\text{c.m.}}$ and orbital angular momentum ℓ is the sum of the quasifission, fusion-fission, and fast-fission cross sections: $\sigma^{\ell}_{\text{cap}}(E_{\text{c.m.}}) = \sigma^{\ell}_{\text{fus}}(E_{\text{c.m.}}) + \sigma^{\ell}_{\text{qfiss}}(E_{\text{c.m.}}) + \sigma^{\ell}_{\text{fast-fis}}(E_{\text{c.m.}})$, where $\sigma^{\ell}_{\text{fus}}(E_{\text{c.m.}}) = \sigma^{\ell}_{\text{ER}}(E_{\text{c.m.}}) + \sigma^{\ell}_{\text{fiss}}(E_{\text{c.m.}})$. We discuss the fusion-fission mechanism and how the branching ratios of these contributions on the beam energy, orbital angular momentum, mass asymmetry parameter of the entrance channel, and the nuclear shell structure of reacting nuclei and their isospin are established. To calculate the evaporation residue cross section correctly, at first, an accurate method must be developed to estimate the fusion probability instead of using the ambiguous fusion cross sections extracted from the experimental data of the mass symmetric fragments when they are assumed to be the genuine fusion-fission yields.

The reactions being studied in this article are massive ones that occur at a dominant role of the quasifission process but they are not so massive to ignore the effect of the orbital angular momentum. Therefore, the calculation method and fusion mechanism are worth presenting. Details of calculations were published in Refs. [7,9,22,32,35,39,40].

The capture cross section is determined by the number of partial waves that lead colliding nuclei to trap into the well of the nucleus-nucleus potential after dissipation of the sufficient part of the initial kinetic energy [Fig. 1(a)]. The size of the potential well decreases by increasing the orbital angular momentum, ℓ. The value of ℓ, at which the potential well disappears, is defined as the critical value ℓ_{cr}. In some models, it is the maximum value of the partial waves giving contribution to the complete fusion. But, unfortunately, this is not true: The use of ℓ_{cr}, as a maximum value of ℓ contributing to capture, leads to the overestimation of the capture and fusion cross sections. Because at $\ell_d < \ell \leqslant \ell_{cr}$ the deep inelastic collisions take place [Fig. 1(b)]. It should be stressed that occurs because of the limited values of the radial friction coefficient [7,12,41], the capture becomes impossible

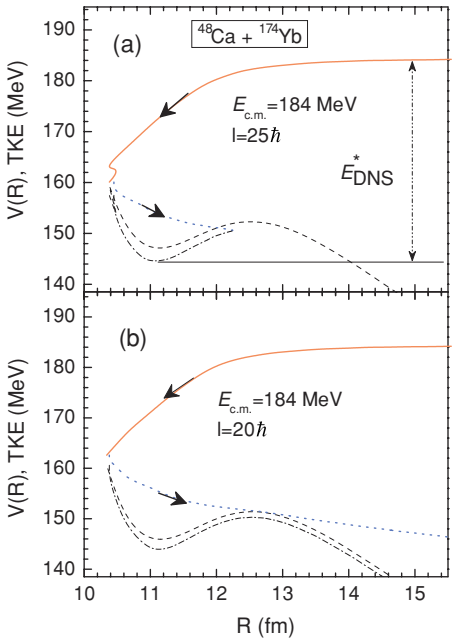

FIG. 1. (Color online) The capture (a) and deep inelastic collisions (b) in the dinuclear system concept. The solid and dotted lines are total kinetic energy (TKE) of the ingoing and outgoing paths of collision, respectively. The dashed and dot-dashed lines are nucleus-nucleus potential $[V(R)]$ for the ingoing and outgoing paths, respectively. $E^*_{\rm DNS}$ is the excitation energy of the dinuclear system formed at capture.

at the low values of the orbital angular momentum if the beam energy values are enough high than the Coulomb barrier.

The capture cross section is calculated by following formula:

$$\sigma_{\rm capture}(E_{\rm c.m.}) = \frac{\lambda^2}{4\pi}\sum_{\ell=0}^{\ell_d}(2\ell+1)\mathcal{P}^{\ell}_{\rm capture}(E_{\rm c.m.}). \qquad (1)$$

Here λ is the de Broglie wavelength of the entrance channel and $\mathcal{P}^{\ell}_{\rm capture}(E_{\rm c.m.})$ is the capture probability that depends on the collision dynamics:

$$\mathcal{P}^{\ell}_{\rm capture}(E_{\rm c.m.}) = \begin{cases} 1 \text{ at } \ell_{\rm min} \leqslant \ell \leqslant \ell_d \\ 0, \text{ if } \ell < \ell_{\rm min} \text{ or } \ell > \ell_d. \end{cases}$$

That means there is a "window" of the ℓ values leading to capture: for example, in calculation of capture in the ^{48}Ca + ^{174}Yb reaction at the beam energy $E_{\rm c.m.} = 184$ MeV, we obtained the "window" with borders $\ell_d = 75\hbar$ and $\ell_{\rm min} = 25\hbar$ for the values of the orbital angular momentum leading to the capture [Fig. 1(a)]. This phenomenon was observed in the ^{64}Ni + ^{100}Mo reaction [42]. At more lower beam energies $\ell_{\rm min}$ moves up to zero and we do not observe the ℓ "window": $0 \leqslant \ell \leqslant \ell_d$.

The fusion cross section is related to the number of events corresponding to the transformation of the dinuclear system into compound nucleus in competition with the quasifission process. It is defined by the product of the partial capture cross section and the related fusion factor $P_{\rm CN}$, which allows one to take into account the competition between the complete fusion and quasifission processes:

$$\sigma^{\ell}_{\rm fus}(E_{\rm c.m.}) = \sigma^{\ell}_{\rm capture}(E_{\rm c.m.})P_{\rm CN}(E_{\rm c.m.}, \ell), \qquad (2)$$

The cross section of evaporation residues formed at each step x of the deexcitation cascade after the emission of the $\nu(x)n + y(x)p + k(x)\alpha + s(x)\gamma$ particles (ν, y, k, and s are numbers of neutrons, protons, α particles, and γ quanta) from the hot CN is calculated by the formula [32,40]:

$$\sigma_{ER(x)}(E^*_x) = \sum_{\ell=0}^{\ell_d}(2\ell+1)\sigma^{\ell}_{(x-1)}(E^*_x)W_{{\rm sur}(x-1)}(E^*_x, \ell), \qquad (3)$$

where $\sigma^{\ell}_{(x-1)}(E^*_x)$ is the partial cross section of the intermediate nucleus formation at the $(x-1)$th step and $W_{{\rm sur}(x-1)}(E^*_x, \ell)$ is the survival probability of the $(x-1)$th intermediate nucleus against fission along the deexcitation cascade of CN; E^*_x is an excitation energy of the nucleus formed at the xth step of the deexcitation cascade. It is clear that $\sigma^{\ell}_{(0)}(E^*_0) = \sigma^{\ell}_{\rm fus}(E^*)$ at $E* = E^*_0 = E_{\rm c.m.} + Q_{gg}$. The numbers of the being emitted neutrons, protons, α particles and γ quanta, $\nu(x)$n, $y(x)$p, $k(x)\alpha$, and $s(x)\gamma$, respectively, are functions of the step x. The emission branching ratios of these particles depend on the excitation energy and angular momentum of the being cooled intermediate nucleus $A = A_{\rm tot} - [\nu(x) + y(x) + 4k(x)]$ and $Z = Z_{\rm tot} - [y(x) + 2k(x)]$.

The analysis and comparison of the measured cross sections of the evaporation residues in the ^{40}Ar + ^{176}Hf [1,2], ^{86}Kr + ^{130}Xe [3], and ^{124}Sn + ^{92}Zr [4] reactions leading to the ^{216}Th* compound nucleus, and the ^{48}Ca + ^{174}Yb [5] and ^{86}Kr + ^{136}Xe [3] reactions leading to the ^{222}Th* compound nucleus require to take into account the capture peculiarities at the initial stage of the reaction. Because the fusion angular momentum distribution is a part of the partial wave set contributing to the capture.

Whether capture occurs or not is found by the solution of the equation of motion for the relative distance R connecting the centers of the reactants and for the orbital angular momentum ℓ taking into account dissipation of the collective kinetic energy [7,9,32,35,39].

The deep-inelastic collision and capture occurring at near and above the Coulomb barrier energies have a similar initial stage up to the turning point, i.e., a collision with the core of the nucleus-nucleus potential. The difference appears at outgoing path after the reflection from the repulsive "core." In deep-inelastic process, the projectile or projectile-like fragment overcomes the Coulomb barrier from the inner part to outside though it loses some part of its kinetic energy, because the friction forces cannot be so intensive so as to cause dissipation of all the relative kinetic energy before overcoming the barrier [Fig. 1(b)]. In the case of capture, this occurs when the projectile or projectile-like fragment cannot overcome the Coulomb barrier from the inner part being trapped into potential well because of the dissipation of its kinetic energy [Fig. 1(a)]. It is clear that the deep inelastic collision occurs at higher energies of the projectile above the Coulomb barrier than in the case of the quasifission for $\ell > \ell_d$ because of using of the friction coefficient with the finite values [41]. Note the radial γ_R and tangential γ_θ friction coefficients, and a change of nucleus-nucleus potential δV and mass of inertia

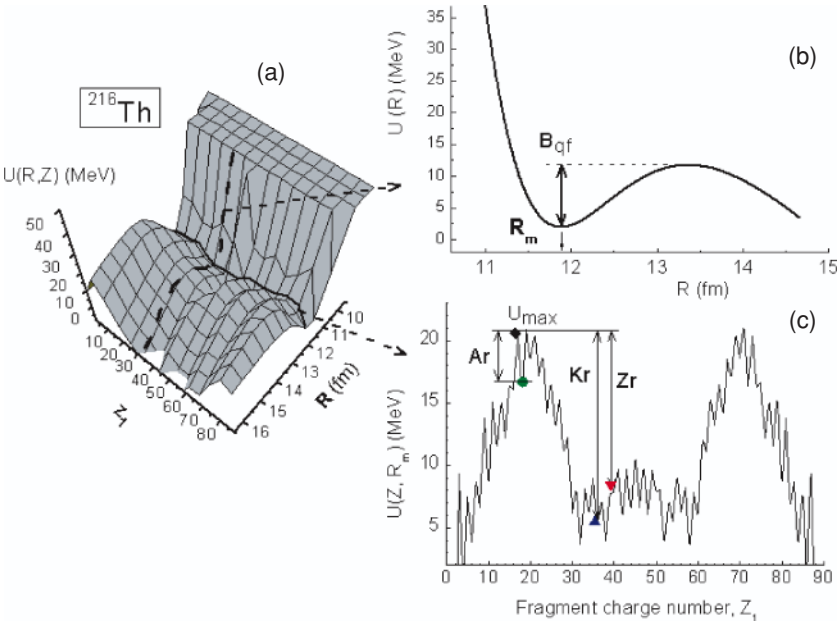

FIG. 2. (Color online) The potential energy surface for a dinuclear system leading to the formation of the ^{216}Th* compound nucleus as a function of the relative distance R and fragment charge number Z_1 (a); the nucleus-nucleus interaction potential $U(R)$ shifted on the Q_{gg} value, and quasifission barrier (B_{qf}) for the ^{86}Kr + ^{130}Xe reaction (b); the driving potential, $U(Z, A, R_m)$, which is the line connecting the minimums of the potential energy surface as a function of Z_1, panel (c). $U_{\max}$ is the maximum value of the driving potential calculated by Eq. (6) using the binding energies from the nuclear data in Ref. [43]. The vertical arrows indicate the intrinsic fusion barrier $B^*_{\rm fus}$ for the ^{40}Ar + ^{176}Hf (Ar, diamond), ^{86}Kr + ^{130}Xe (Kr, up triangle), and ^{124}Sn + ^{92}Zr (Zr, down triangle) reactions leading to ^{216}Th.

$\delta\mu$ for the relative motion are found from the calculations of the nucleon exchange and particle-hole excitations in nuclei [7,23,41].

The amount of energy above the Coulomb barrier determines what of these two processes occurs. If capture occurs, then we calculate the competition between quasifission and complete fusion.

According to this scenario the complete fusion and quasifission are considered as a diffusion process along the mass symmetry axis and relative distance between the centers of nuclei, respectively, after the formation of the dinuclear system. Therefore, the quasifission is considered as a quasistationary process [18] and the statistical approach can be used to calculate the fusion probability $P_{\rm CN}(E_{\rm c.m.}, \ell)$ [a factor in Eq. (2)]. The large difference between the measured excitation functions of the ^{86}Kr + ^{130}Xe and ^{124}Sn + ^{92}Zr reactions at small differences of values of charge asymmetry and Z_1Z_2 for these reactions stimulates us to improve the calculation method of $P_{\rm CN}$ by taking into account the DNS evolution on the charge asymmetry axis. Competition between complete fusion and quasifission takes place for all possible configurations of DNS: Z_1 and $Z_{\rm tot} - Z_1$.

During the formation of the dinuclear system at the capture stage there is an intense nucleon exchange between reacting nuclei. In the quasifission and fusion processes, an intense mass transfer takes place and, in dependence on the entrance channel, the mass asymmetry degree of freedom may be fully or partially equilibrated [15]. As a result, while DNS exists, we have an ensemble $\{Z\}$ of the DNS configurations that contributes to the competition between complete fusion and quasifission with the probabilities $\{Y_Z\}$. Position of the maximum of the mass distribution is determined by the peculiarities of the nuclear shell structure and lifetime of the dinuclear system [35]. Calculations have been performed by the solution of the equation for the distribution function for the charge asymmetry of the dinuclear system fragments. Therefore, the statistical calculation of $P_{\rm CN}(E^*_{\rm DNS}, \ell)$ is performed by the formula:

$$P_{\rm CN}(E^*_{\rm DNS}, \ell) = \sum_{Z_{\rm sym}}^{Z_{\max}} Y_Z(E^*_{\rm DNS}, \ell) P^{(Z)}_{\rm CN}(E^*_{\rm DNS}, \ell) \qquad (4)$$

where the intrinsic fusion $B^*_{\rm fus}$ and quasifission $B_{\rm qf}$ barriers which are found from the driving potential and potential well, respectively (see Fig. 2); $Z_{\rm sym} = (Z_1 + Z_2)/2$; $Z_{\max}$ corresponds to the charge asymmetry where the driving potential reaches its maximum $[B^*_{\rm fus}(Z_{\max}) = 0]$ (see Refs. [22,23]):

$$P^{(Z)}_{\rm CN} = \frac{\rho[E^*_{\rm DNS}(Z) - B^*_{\rm fus}(Z)]}{\rho[E^*_{\rm DNS}(Z) - B^*_{\rm fus}(Z)] + \rho[E^*_{\rm DNS}(Z) - B_{\rm qf}(Z)]}, \qquad (5)$$

where $\rho[E^*_{\rm DNS}(Z) - B^*_K(Z)]$ is the DNS level density calculated on the quasifission and intrinsic fusion barriers ($B_K = B_{\rm qf}, B^*_{\rm fus}$) and $Y_Z(E^*_{\rm DNS}, \ell, t)$ is the probability of population of the DNS configuration $(Z, Z_{\rm tot} - Z)$ at $E^*_{\rm DNS}(Z)$ and ℓ. The evolution of Y_Z is calculated by solving the transport master equation with the transition coefficients of the multinucleon transfer which were determined in Refs. [40,44]. For more details see Ref. [40].

Both characteristics of the fusion excitation function, namely its maximum value and width (energy window for the complete fusion) are related by the ratio between $B^*_{\rm fus}$ and $B_{\rm qf}$ for the given reaction.

In Fig. 2(a), the driving potential $U(Z, A, R_m, \ell)$ for the dinuclear systems of the reactions leading to ^{216}Th* CN is presented. It is determined from the landscape of the potential energy surface $U(A, Z; R, \ell)$:

$$\begin{aligned} U(A, Z; R, \ell) &= U(A, Z, \ell, \beta_1, \alpha_1; \beta_2, \alpha_2) \\ &= B_1 + B_2 + V(Z, \ell, \beta_1, \alpha_1; \beta_2, \alpha_2; R) \\ &\quad - [B_{\rm CN} + V_{\rm CN}(\ell)]. \end{aligned} \qquad (6)$$

Here, B_1, B_2, and $B_{\rm CN}$ are the binding energies of the constituents of the DNS and of the CN, respectively, which were obtained from Refs. [43,45]; β_i are the fragment deformation parameters and α_i are the orientations relative to the beam direction. The quadrupole (2^+) and octupole (3^-) collective excitations in spherical nuclei are taken into account. The values of $\beta_2^{(2^+)}$ (taken from Ref. [46]) and the ones of $\beta_3^{(3^-)}$ (taken from Ref. [47]) were used as the static deformations in calculation of the nucleus-nucleus potential.

The distribution of neutrons between the DNS constituents for the given proton numbers Z and Z_2 or ratios A/Z and A_2/Z_2 for both fragments ($A = A_1$, $A_2 = A_{\rm tot} - A$, $A_{\rm tot}$ is the mass number of the dinuclear system) were determined by minimizing the potential $U(A, Z; R, \ell)$ for each Z. $B^*_{\rm fus}(Z)$ is determined by the difference between the maximum value of the driving potential $U(Z, A, R_m)$ and its value at the given charge asymmetry Z [see Fig. 2(c)]. The quasifission barrier ($B_{\rm qf}$) is defined by the depth of well of $U(Z, R)$ [22,23] for the given charge asymmetry Z [Fig. 2(b)].

The values of $U(Z, A, R_m, \ell)$ is found from the potential energy surface $U(A, Z; R, \ell)$ as a line lying on the bottom of the valley along the charge asymmetry axis [Fig. 2(c)]. R_m is the position of its minimum value $U(Z, A, R_m, \ell)$ being function of R for the given charge number Z [Fig. 2(b)]. This minimum corresponds to the bottom of the potential well and its position on the R axis is marked by $R = R_m$.

The shapes of the potential energy surface and driving potential depend on the orientations of nuclei relative to the axis connecting the centers of interacting nuclei [9]. For example, the driving potential in Fig. 2(c) is calculated for the orientation angles $\alpha_1 = 45^\circ$ and $\alpha_1 = 30^\circ$ of the projectile and target symmetry axes, respectively. In this figure $B^*_{\rm fus}$ is shown for the ^{40}Ar + ^{174}Hf, ^{86}Kr + ^{130}Xe, and ^{124}Sn + ^{92}Zr reactions. If the excitation energy of the dinuclear system, $E^*_{\rm DNS} = E_{\rm c.m.} - V(R_m, \ell)$, is not enough to overcome $B^*_{\rm fus}$, then the dinuclear system may immediately decays into two fragments or its decay occurs after multinucleon transfer from heavy fragment into light one. Both of decays are called quasifission. So, quasifission fragments can be of different mass asymmetry. Therefore, quasifission occurs because of the motion along the relative internuclear distance R and DNS should overcome the barrier ($B_{\rm qf}$) defined by the depth of well of $V(R)$ [see Fig. 2(b)]. This phenomenon takes place in reactions with massive nuclei of symmetric masses. The advantage of the model under discussion is that it allows us to show the importance of such characteristics of the entrance channel as the mass and charge of the colliding nuclei, their shape and shell structure, the beam energy and orbital angular momentum.

The potential energy surface $U(A, Z; R, \ell)$ [Eq. (6)] is calculated as a function of the charge number $Z = Z_1$ of one of the dinuclear system constituents ($Z_2 = Z_{\rm tot} - Z$, $Z_{\rm tot}$ is the charge of DNS). In Refs. [48,49], authors applied the Fokker-Planck equation to analyze the quasifission and complete fusion considering them as a diffusion process. They obtained a formula $P_{\rm CN}$ as a ratio of the quasistationary rates of fusion Λ_η and quasifission Λ_R through the intrinsic fusion barrier ($B_\eta = B^*_{\rm fus}$) in $\eta = |A_1 - A_2|/(A_1 + A_2)$ and the quasifission barrier ($B_R = B_{\rm qf}$) in R, respectively. We

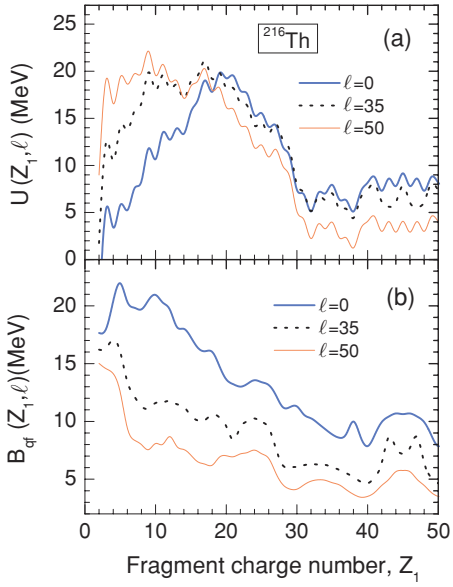

FIG. 3. (Color online) The driving potential (a) and quasifission barrier (b) for the dinuclear system formed in the reactions leading to the ^{216}Th* compound nucleus as a function of the charge number of its light constituent calculated for the three values of orbital angular momentum: $\ell(\hbar) = 0$ (thick line), 35 (dotted line), and 50 (thin line).

should note that the method used in this article and the one developed in Refs. [48,49] give close results for the fusion probability in the "cold reactions" on the ^{208}Pb target (Refs. [7] and [49]) and "warm reactions" with the ^{48}Ca projectile (Refs. [22] and [50]). The both methods showed that the barriers $B_{\rm qf}$ and $B^*_{\rm fus}$ play a main role in the competition between quasifission and complete fusion.

It is seen from Fig. 3 that the values of the $B_{\rm qf}$ and $B^*_{\rm fus}$ for the dinuclear system formed in reactions leading to ^{216}Th change in opposite directions as a function of the orbital angular momentum ℓ: the quasifission barrier $B_{\rm qf}$ decreases and the intrinsic fusion barrier $B^*_{\rm fus}$ increases by the increase of ℓ. Therefore, the fusion probability $P_{\rm CN}$, being a function of these barriers $B^*_{\rm fus}$ and $B_{\rm qf}$ decreases with increasing ℓ at given values of the beam energy. An advantage of this way of calculation is that it allows us to have the partial fusion cross section, i.e., the fusion angular momentum distribution that shows the effect of the entrance channel.

For instance, the drastic decrease of the cross section of the synthesis of superheavy elements is explained by the interrelation among $B^*_{\rm fus}$, $B_{\rm qf}$, and $E^{*(\rm max)}_{\rm DNS}$. It is seen from Fig. 4 that the dependence of these quantities on the charge (and mass) of the compound nucleus is strong: the intrinsic fusion barrier $B^*_{\rm fus}$ increases and the quasifission barrier decreases gradually with the atomic number of the projectile (^{50}Ti, ^{58}Fe, ^{64}Ni, ^{70}Zn, ^{86}Kr) when the same target nucleus (^{208}Pb or ^{209}Bi) is used.

The maximum value of the possible excitation energy $E^{*(\rm max)}_{\rm DNS}$ of the dinuclear system is determined by the difference between the largest initial beam energy leading to the formation of the DNS (capture) and the minimum of the well bottom of the nucleus-nucleus potential $V(R)$. In turn, for

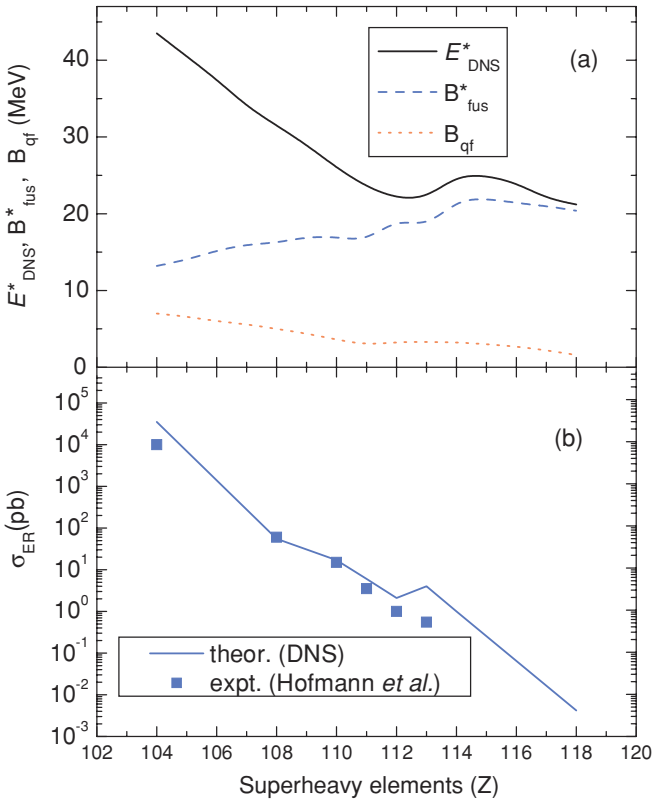

FIG. 4. (Color online) The dependence of the excitation energy $E^{*(\max)}_{\rm DNS}$ (solid line), intrinsic fusion barrier $B^{*}_{\rm fus}$ (dashed line), and quasifission barrier $B_{\rm qf}$ (dotted line) of the dinuclear system (a), and the maximum of the evaporation cross sections (b) on the charge number of the superheavy elements in the "cold" fusion reactions (squares are the experimental data of the GSI experiments [51] and solid line is the result of our calculations) (b).

the given potential well, the largest initial beam energy at which the capture occurs depends on the friction coefficient. In the model [41], the friction coefficients are determined by the intense nucleon exchange between reacting nuclei and particle-hole excitations in them. The kinetic energy of the collision is transformed into excitation energy of the nuclei because of the interaction of the motion of nucleons inside the nuclei and nucleon exchange between them. The maximum value $E^{*(\max)}_{\rm DNS}$ decreases when the size of the potential well becomes smaller that takes place by increasing of Z_1Z_2. As a result, for a heavy system such as ^{86}Kr + ^{208}Pb, the fusion cross section decreases drastically and the amalgamation of nuclei becomes more difficult. Because, in this case, the intrinsic fusion barrier $B^{*}_{\rm fus}$ is so high and the quasifission barrier $B_{\rm qf}$ is so low that dinuclear system has a negligible chance to be fused into ^{294}118.

III. COMPARISON OF CALCULATED RESULTS AND EXPERIMENTAL DATA

The difference between the measured data on the cross section of evaporation residues for the ^{40}Ar + ^{176}Hf [1,2], ^{86}Kr + ^{130}Xe [3], and ^{124}Sn + ^{92}Zr [4] reactions leading to the heated ^{216}Th* CN, as well as that for the ^{48}Ca + ^{174}Yb [5] and ^{86}Kr + ^{136}Xe [3] reactions leading to the heated ^{222}Th* CN, are explained by the dependencies of fusion excitation functions on the mass asymmetry and shell structure of colliding nuclei and by the dependencies of the survival probabilities $W_{\rm sur}(E^*, \ell)$ on the $\sigma^{\ell}_{\rm fus}(E^*)$ dependence of the excited compound nuclei produced in these reactions. Obviously, the yields of the evaporation residues produced along the steps of the deexcitation cascade of CN strongly depend on the angular momentum distributions of the intermediate excited nuclei formed in the different reactions (see Figs. 8 and 9 of the article reported in Ref. [32]).

A. The reactions leading to ^{216}Th*

A dependence of the reaction mechanism on the entrance channel was observed in experiments with reactions leading to the same compound nucleus. The experimental data reveal that the maximum value of the $\sigma_{\rm ER}(E_{\rm c.m.})$ for ^{40}Ar + ^{176}Hf (I) [1,2] is 12 times larger than for ^{86}Kr + ^{130}Xe (II) [3] and 3 times larger than for ^{124}Sn + ^{92}Zr (III) [4] (see Fig. 5). The ^{40}Ar + ^{176}Hf reaction has a larger charge asymmetry $[\eta_Z = |Z_2 - Z_1|/(Z_1 + Z_2)]$ in comparison with the two others (II,III). This result agrees with the conclusions of the macroscopic dynamical model (MDM) [52] and DNS models which state that more asymmetric reactions are favorable for the formation of a massive compound nucleus. In MDM, the extra-extra push energy E_{xx}, which is needed to transform a dinuclear system into the compound nucleus, is smaller for an asymmetric reaction than that for a more symmetric one leading to the same compound nucleus because

$$Z_1^{\rm asym} Z_2^{\rm asym} < Z_1^{\rm sym} Z_2^{\rm sym},$$

where is $Z_1^{\rm asym} + Z_2^{\rm asym} = Z_1^{\rm sym} + Z_2^{\rm sym}$. The calculated driving potential by the DNS model shows that the barrier $B^{*}_{\rm fus}$ on the way to fusion (on the mass asymmetry axis) is smaller for the asymmetric reaction than that for the symmetric one, whereas the quasifission barrier is larger for a more asymmetric reaction (see Table I), and as a result the fusion factor $P_{\rm CN}$ becomes larger in this case. As shown in Figs. 5(a) and 5(b), the excitation functions of the capture and fusion for the reaction (I) is higher than that for the reactions (II) and (III) at high E^* values (at about $E^* > 56$ MeV), because the potential well of the entrance channel for the reaction (I) is deeper than that for the others. Therefore, $B^{(\rm I)}_{\rm qf} > B^{(\rm II)}_{\rm qf}, B^{(\rm III)}_{\rm qf}$ (see Table I), whereas the smallness of $B^{*}_{\rm fus}$ for the reaction (I) is connected with the peculiarities of the driving potential [Fig. 2(c)]. At lower energies E^* ($E^{*}_{\rm DNS} < 56$ MeV), the capture cross section for the ^{40}Ar + ^{176}Hf reaction is lower than the ones of the reactions (II) and (III) because of the difference of their Q_{gg} values: the reaction (I) starts from a higher E^* value (namely at about 28 MeV), whereas the capture cross section of the reactions (II) and (III) can reach lower E^* values ($E^{*}_{\rm DNS}$ about 12 MeV).

The evaporation residue excitation functions calculated in this article are in good agreement with the experimental data [see Fig. 5(c)]. It is seen from Fig. 5(c) that the maximum value of the ER cross section measured for the ^{86}Kr + ^{130}Xe

TABLE I. Charge asymmetry, intrinsic fusion ($B^*b_{\rm fus}$), and quasifission ($B_{\rm qf}$) barriers, and the fusion factor ($P_{\rm CN}$) for the reactions leading to the ^{216}Th* CN.

Reactions	η_Z	$B^*_{\rm fus}$ (MeV)	$B_{\rm qf}$ (MeV)	$P_{\rm CN}$
^{40}Ar + ^{176}Hf (I)	0.63	4.54	15.42	0.421
^{86}Kr + ^{130}Xe (II)	0.20	14.70	8.82	0.006
^{124}Sn + ^{92}Zr (III)	0.15	11.81	8.25	0.048

reaction is 4 times smaller than that for ^{124}Sn + ^{92}Zr near the same value of $E^*_{\rm CN}$, though the former reaction is more asymmetric ($\eta_Z = 0.20$) than the latter one ($\eta_Z = 0.15$). This result is explained by the driving potential calculated using the binding energies obtained from the mass table [43]. As one can see in Fig. 2(c), $B^*_{\rm fus}$ for the ^{86}Kr + ^{130}Xe (II) reaction is larger (14.70 MeV) than the one of the ^{124}Sn + ^{92}Zr (III) reaction (11.81 MeV), whereas the quasifission barriers for the (II) and (III) reactions are comparable and equal to 8.82 and 8.25 MeV, respectively. The relatively smallness of $B^*_{\rm fus}$ for the reaction (III) is caused by the shell effects contained in the nuclear binding energy that form a bump in the charge symmetric region $(Z_1 + Z_2)/2 \pm 8$ of the driving potential [Fig. 2(c)].

The dependence of $B^*_{\rm fus}$ on the orbital angular momentum (Fig. 3) affects the partial fusion cross sections (Fig. 6). It is seen from the comparison of the driving potentials calculated for the three different values of the initial angular momentum ℓ that $B^*_{\rm fus}$ increases (top panel of Fig. 3) and $B_{\rm qf}$ decreases (bottom panel of Fig. 3) via the increase of ℓ. For example, for the (II) reaction the intrinsic fusion barrier $B^*_{\rm fus}$ is about 14.7 MeV for $\ell = 0$ and it increases up to 19.7 MeV for $\ell = 50\hbar$ (see top panel of Fig. 3), whereas the quasifission barrier $B_{\rm qf}$ decreases from 8.8 MeV (for $\ell = 0$) to 4.2 MeV for $\ell = 50\hbar$ (see bottom panel of Fig. 3). As a result the fusion factor $P_{\rm CN}$ decreases by increasing the orbital angular momentum ℓ. For the more symmetric reactions this effect appears more strongly. Therefore, the partial fusion cross section in the reaction (I) against the excitation energy E^* of CN (top panel of Fig. 6) has a larger volume under the surface of $\sigma^\ell_{\rm fus}(E^*)$ in comparison with the reactions (II) (middle panel) and (III) (bottom panel). But the volume of the $\sigma^\ell_{\rm fus}(E^*)$ distribution corresponding to the reaction (III) is larger than that for the reaction (II). This is a result of the dependence of the partial fusion cross sections $\sigma^\ell_{\rm fus}(E^*)$ (2) on the intrinsic

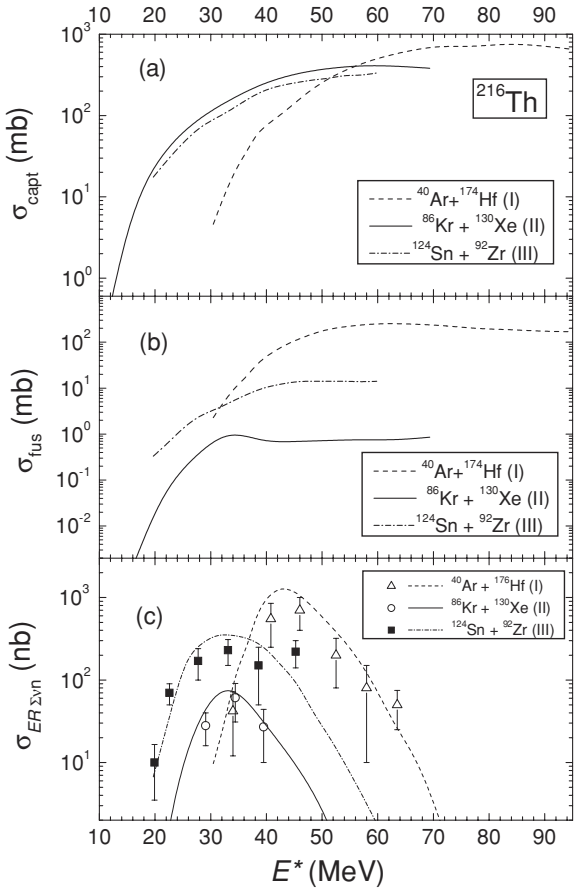

FIG. 5. Comparison of the calculated capture (a), fusion (b), and evaporation residue (c) excitation functions as well as the measured excitation functions of evaporation residue (c) for the ^{40}Ar + ^{176}Hf (dashed line and open up triangles [1,2]), ^{124}Sn + ^{92}Zr (dash-dotted line and solid squares [4]), and ^{86}Kr + ^{130}Xe (full line and open circles [3]) reactions leading to the ^{216}Th* CN.

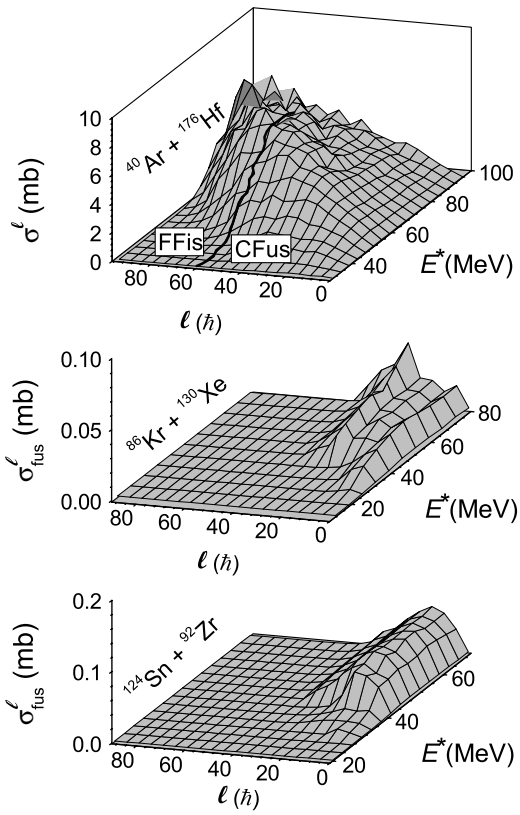

FIG. 6. The calculated angular momentum distributions of the compound nucleus $[\sigma^\ell_{\rm fus}(E^*)]$ formed in the ^{40}Ar + ^{176}Hf (top panel), ^{86}Kr + ^{130}Xe (middle), and ^{124}Sn + ^{92}Zr (bottom) reactions at various excitation energy E^* values. In the top panel, the full thick line (corresponding to the disappearance of the fission barrier) separates the complete fusion contribution (CFus) from the fast-fission contribution (FFis).

fusion barrier that is smaller for the reaction (III) than for the reaction (II).

From the analysis of these (I, II, and III) reactions leading to ^{216}Th*, one can conclude the following:

(i) The influence of such peculiarities of the entrance channel as mass (charge) asymmetry and shell structure of the reactants on the competition between fusion and quasifission and on the fusion-fission mechanism is strong.

(ii) The difference between fusion excitation functions deals with the values of $B^*_{\rm fus}$ and $B_{\rm qf}$, which depends on the peculiarities of the shell structure and shape of nuclei.

(iii) Because of the large difference between the Q_{gg} values of these three reactions leading to the ^{216}Th* CN, the centers of their excitation functions (see Fig. 5) are placed at different values of the excitation energy.

Despite the ^{124}Sn + ^{92}Zr (III) reaction being more mass symmetric ($\eta_A = 0.148$) than the ^{86}Kr + ^{130}Xe (II) reaction ($\eta_A = 0.204$), the cross sections of the evaporation residue formation for the mass symmetric reaction (III) is larger than that for the (II) reaction [Fig. 5(c)] because the realistic driving potential has a big bump (see Fig. 3), leading to a decrease of the intrinsic fusion barrier $B^*_{\rm fus}$, because of the peculiarities of the nuclear shell structure in the ^{216}Th* CN.

In these reactions under consideration, the evaporation residue cross sections are several orders of magnitude smaller than the fission cross sections (Fig. 5). It means that the fission cross section is approximately equal to the fusion cross section. The comparison of the calculated fusion excitation function with the data of mass symmetric fragments is intriguing at investigation of the mechanism of the fusion-fission reactions. This has been done for the ^{40}Ar + ^{176}Hf reaction (Fig. 7). In Ref. [2], the authors assumed that the fission cross section is equal to the fusion cross section restored from the experimental data on the yield of symmetric mass fragments at the complete

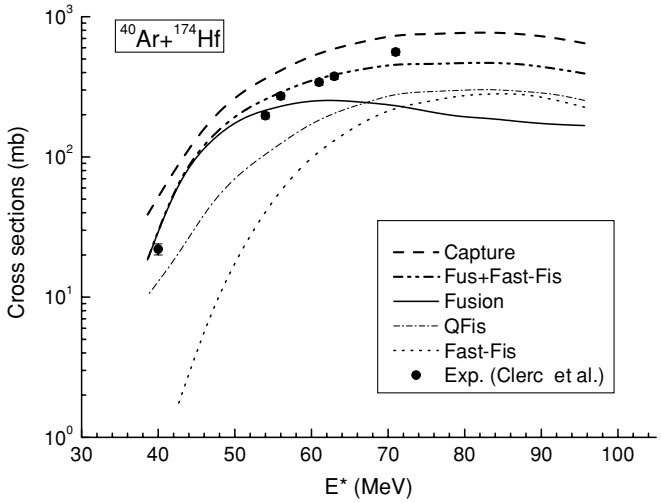

FIG. 7. Comparison of the calculated capture (dashed line), fusion (solid line), quasifission (dot-dashed line), and fast-fission (dotted line) excitation functions with the experimental data (full circles) of the two symmetric mass fragments for the ^{40}Ar + ^{176}Hf reaction [2]. The double dot-dashed line is the sum of the fusion and fast-fission cross sections.

momentum transfer. It should be stressed that those products could be formed not only at the fission of a hot CN but also at quasifission of a DNS that lives long enough to reach mass equilibration or at the fast-fission process, if the DNS being transformed into a mononucleus has an angular momentum ℓ higher than $60\hbar$ (see top panel in Fig. 6). Because starting from this value of ℓ the fission barrier of ^{216}Th* disappears [21]. Experimentally it is difficult to distinguish the fission fragments of the compound nucleus from the products of the quasifission of DNS and fast fission of the mononucleus at $\ell > \ell_f$ where there is not barrier providing its stability. In Ref. [12], the calculations showed that the contribution of the quasifission increases with the beam energy above the fusion barrier. For example, in Fig. 7, we compare the calculated capture, fusion, quasifission, and fast-fission excitation functions with the data [2] of the mass symmetric fragments for the ^{40}Ar + ^{176}Hf reaction. The underestimation of the experimental data at $E^* > 56$ MeV by our fusion cross sections means that there are contributions from quasifission and fast-fission fragments that could be considered the fusion-fission products (Fig. 7). As shown, the sum of the fusion and fast-fission cross sections (double dot-dashed line in Fig. 7) is in good agreement with the data of the symmetric mass fragments. Because the products of the fast-fission process can be registered as the fusion-fission products, whereas the quasifission process contributes more to the mass asymmetric region than the mass symmetric one. Therefore, the sum of the fusion and fast-fission cross sections have been compared with the data of the symmetric mass fragments. We remind that the capture cross section is the sum of the fusion, quasifission, and fast-fission cross sections.

B. The reactions leading to ^{222}Th*

The maximum of the experimental excitation functions of evaporation residues for ^{48}Ca + ^{174}Yb (IV) [5] is higher than that for ^{86}Kr + ^{136}Xe (V) [3] [Fig. 8(c)]. This fact is explained by the larger fusion cross section of the ^{48}Ca + ^{174}Yb reaction in comparison with that of the ^{86}Kr + ^{136}Xe reaction [Fig. 8(b)]. The difference between them reaches more than 1 order of magnitude for $E^* > 45$ MeV though at $E^* < 45$ MeV the capture cross section of the ^{48}Ca + ^{174}Yb (IV) reaction is lower than that for the ^{86}Kr + ^{136}Xe (V) reaction. This last result is related to the difference between Q_{gg} values for these reactions: $Q_{gg} = -118.35$ MeV for the reaction (IV) and $Q_{gg} = -186.88$ MeV for the ^{86}Kr + ^{136}Xe (V) reaction. That allows the capture cross section of the reaction (IV) to start from E^* about 20 MeV, whereas the capture cross section for the (V) reaction reaches lower excitation energies (up to $E^*_{\rm DNS}$ about 10 MeV).

In Table II, we report the values of the charge asymmetry parameter, intrinsic fusion barrier, and quasifission barrier for such two reactions leading to the ^{222}Th* CN.

By comparing the two reactions leading to the ^{222}Th* CN, increasing the excitation energy E^*, we find a higher probability of the fission process for the ^{48}Ca + ^{174}Yb reaction caused by the $\sigma^\ell_{\rm fus}(E^*)$ distribution. As one can see, the $\sigma^\ell_{\rm fus}(E^*)$ dependence of CN formed in the ^{48}Ca + ^{174}Yb reaction against

TABLE II. Charge asymmetry, intrinsic fusion (B^*_{fus}), and quasifission (B_{qf}) barriers and the fusion factor (P_{CN}) for the reactions leading to the ^{222}Th* CN.

Reactions	η_Z	B^*_{fus} (MeV)	B_{qf} (MeV)	P_{CN}
^{48}Ca + ^{174}Yb (IV)	0.56	8.73	9.18	0.270
^{86}Kr + ^{136}Xe (V)	0.20	9.04	7.64	0.016

the excitation energy (Fig. 9, top panel) has a larger volume than that of the ^{86}Kr + ^{136}Xe reaction (bottom panel).

The analysis of the ^{48}Ca + ^{174}Yb and the ^{86}Kr + ^{136}Xe reactions leading to the ^{222}Th* CN shows that the influence of the mass asymmetry and peculiarities of the shell structure on the competition between fusion and quasifission mechanism is strong. Nevertheless, the comparison of the measured data on the evaporation residue cross sections for the two considered reactions does not reflect directly the role of the mass asymmetry of the entrance channel. The large difference between the fusion cross sections was compensated by the different fission probability of nuclei formed in these reactions at various steps of deexcitation cascade of ^{222}Th*. For example, at $E^* = 35$ MeV of CN, the average fission probability Γ_f/Γ_{tot} of each nucleus for the first five steps of the deexcitation cascade is 0.62 for ^{222}Th* obtained in the

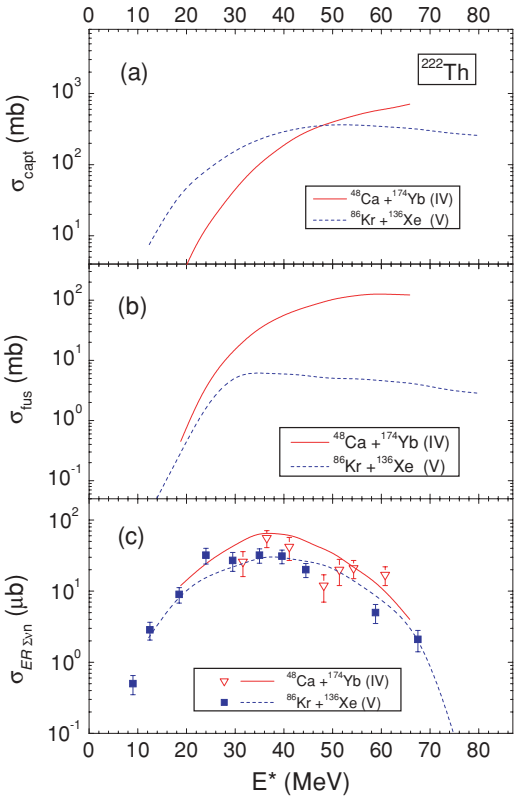

FIG. 8. (Color online) Comparison of the calculated (lines) capture (a), fusion (b), and evaporation residue (c) excitation functions as well as the measured (symbols) excitation functions of evaporation residue (c) for ^{48}Ca + ^{174}Yb [5] (solid curve and open down triangles) and ^{86}Kr + ^{136}Xe [3] (dashed curve and solid squares) reactions leading to ^{222}Th*.

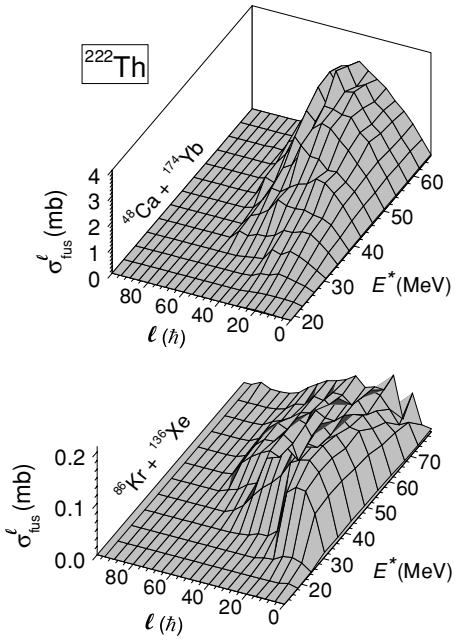

FIG. 9. The calculated angular momentum distributions of compound nucleus [$\sigma^{\ell}_{fus}(E^*)$] formed in the ^{48}Ca + ^{174}Yb (top panel) and ^{86}Kr + ^{136}Xe (bottom panel) reactions at various excitation energy E^* values of CN.

^{48}Ca + ^{174}Yb (IV) reaction, whereas this ratio is 0.53 for the cascade of CN reached by the ^{86}Kr + ^{136}Xe (V) reaction. At $E^* = 65$ MeV of CN, the average fission probability calculated for the first seven steps of the cascade is 0.57 for the reaction (IV), whereas it is 0.34 for the reaction (V). This result is because of different distributions of the orbital angular momentum of CN (see Fig. 9) reached by the different projectile-target combinations.

C. Comparison of reactions induced by ^{86}Kr on the ^{130}Xe and ^{136}Xe targets

Another interesting phenomenon that was observed in the comparison of the experimental data for reactions induced by the ^{86}Kr projectile on the ^{130}Xe and ^{136}Xe targets is that the measured ER cross section in ^{86}Kr + ^{130}Xe (II) (forming the ^{216}Th* CN) is about 500 times smaller than that measured in ^{86}Kr + ^{136}Xe (V) (forming the ^{222}Th* CN). In Fig. 10(c), the experimental and theoretical excitation functions of the total evaporation residue cross sections for the neutron emission only along the deexcitation cascade of the ^{216}Th* and ^{222}Th* CN formed in the above-mentioned reactions are compared. It is clear that the differences between the excitation functions are caused by the excess number of neutrons in the ^{136}Xe target in comparison with the ^{130}Xe one. Moreover, the higher values of the fusion cross section for the reaction with the ^{136}Xe target, in respect to the lower values of the fusion cross section for the reaction with the ^{130}Xe target, is also in agreement with the role of the mass asymmetry that is higher for the ^{86}Kr + ^{136}Xe reaction [η_A is 0.225 for the (V) reaction, whereas it is 0.204 for the (II) reaction].

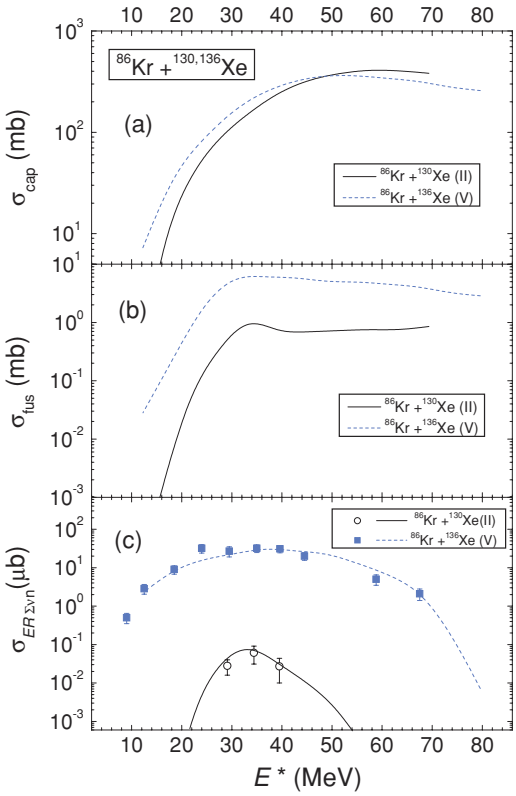

FIG. 10. (Color online) Comparison of the calculated capture (a), fusion (b), and evaporation residue (c) excitation functions (lines) as well as the measured excitation functions (symbols) of evaporation residue (c) for the ^{86}Kr + ^{136}Xe [3] (solid line and solid squares) and ^{86}Kr + ^{130}Xe [3] (dashed line and open circles) reactions.

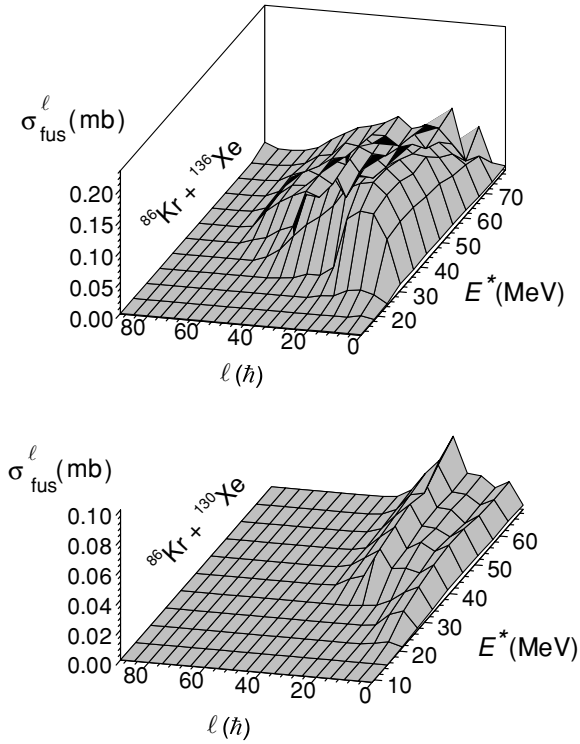

FIG. 11. Comparison of the calculated angular momentum distributions $\sigma^{\ell}_{fus}(E^*)$ for the ^{86}Kr + ^{136}Xe (top panel) and ^{86}Kr + ^{130}Xe (bottom panel) reactions at various excitation energy E^* values of ^{222}Th* and ^{216}Th*, respectively.

Also the ratio between the values of the fusion cross sections for the two above-mentioned reactions is in agreement with the values of the B^*_{fus}/B_{qf} ratio obtained for the reactions under consideration. The B^*_{fus}/B_{qf} value is 1.18 for the (V) reaction, whereas the ratio is 1.67 for the (II) reaction; therefore, a lower value of the B^*_{fus}/B_{qf} ratio stimulates a higher rate of the complete fusion formation in competition with the quasifission process.

As a result we find the following two characteristics for the fusion-fission mechanism of the two reactions under consideration:

(i) The fusion cross section calculated by the model based on the DNS concept [7,12] for the ^{86}Kr + ^{130}Xe (II) reaction is much smaller than that for the ^{86}Kr + ^{136}Xe (V) reaction [Fig. 10(b)]. Therefore, the volume of the $\sigma^{\ell}_{fus}(E^*)$ distribution formed in the (II) reaction is smaller than that for the (V) reaction (see Fig. 11). This result is because of the fact that the intrinsic fusion barrier B^*_{fus} and the B^*_{fus}/B_{qf} ratio are smaller for the ^{86}Kr + ^{136}Xe reaction than the corresponding values for the ^{86}Kr + ^{130}Xe reaction (see the values of barriers presented in Tables I and II), stimulating the more high rate for the fusion in the reaction (V).

(ii) The survival probability W_{sur} decreases along the steps of the ^{216}Th* deexcitation cascade, whereas W_{sur} increases along the steps of the ^{222}Th* cascade. This behavior is because of the shell corrections, which, on average, decrease for the intermediate excited nuclei after $1n, 2n \ldots xn$ emissions from ^{216}Th*, increasing the fission probability and decreasing the probability of the ER formation; whereas, the shell corrections in the intermediate excited nuclei, which are formed after the analogous neutron emission from ^{222}Th*, increase leading to the increase of the probability of the ER formation because of approaching to the closed shell $N = 126$. Moreover, at each step ($1n$, $2n$, $3n$ $\ldots$ xn) of the deexcitation cascade of the initial compound nucleus, the neutron separation energy S_n at each step of the ^{222}Th* decay chain is about 1–2 MeV lower than that at the analogous step of the neutron emission from ^{216}Th*. By comparing the Γ_n/Γ_f values at each step of the cascade of ^{222}Th* and ^{216}Th*, at the same excitation energy of the CN, we find that the $(\Gamma_n/\Gamma_f)_{^{222}\mathrm{Th}*}$ ratios are always much larger than the $(\Gamma_n/\Gamma_f)_{^{216}\mathrm{Th}*}$ ones. Because large Γ_n/Γ_f values correspond to a large evaporation residue cross section, the excess number of neutrons increases the survival probability in the ^{86}Kr + ^{136}Xe reaction in comparison with the ^{86}Kr + ^{130}Xe one.

IV. CONCLUSIONS

The role of the entrance channel in the fusion-fission reactions was studied intending to account for the difference between the experimental data for the ^{40}Ar + ^{176}Hf [1,2], ^{86}Kr + ^{130}Xe [3], and ^{124}Sn + ^{92}Zr [4] reactions leading to the ^{216}Th* compound nucleus, and the ^{48}Ca + ^{174}Yb [5],

^{86}Kr + ^{136}Xe [3] reactions leading to the ^{222}Th* compound nucleus. The results of calculations, in the framework of the DNS concept [7,10,40] for the fusion cross sections, and the advanced statistical model [36–38,40] for the total evaporation residue cross sections, have been compared with the measured experimental data for these reactions. From the analysis of the experimental data four phenomena were studied:

(i) Among reactions leading to ^{216}Th*,^{40}Ar + ^{176}Hf has more larger evaporation residues in comparison with two others: ^{86}Kr + ^{130}Xe and ^{124}Sn + ^{92}Zr. This result confirms conclusions of macroscopic dynamical and DNS models that state that more asymmetric reactions are favorable for the formation of the massive compound nucleus. For the reactions leading to the same compound nucleus, the extra-extra push energy E_{xx} in MDM [52] (which is needed to transform the dinuclear system into compound nucleus) and the intrinsic fusion barrier $B^*_{\rm fus}$ in the DNS concept (both of them are a hindrance to the fusion) are smaller for an asymmetric reaction than for a more symmetric one [Fig. 2(c)].

(ii) As an exclusion from the regularity in (i) an unexpected phenomenon was observed: the measured maximum value of the ER cross section for ^{86}Kr + ^{130}Xe (II) is 4 times smaller than that for ^{124}Sn + ^{92}Zr (III), nearly at the same E^* value. This result is in opposite tendency to the general conclusions of MDM and DNS models. The observed difference between the excitation functions of evaporation residues for the ^{86}Kr + ^{130}Xe and ^{124}Sn + ^{92}Zr reactions is explained by the difference of $B^*_{\rm fus}$, which is seen from the driving potential calculated for these reactions using experimental binding energies of fragments [43]. As one can see in Fig. 2(c), $B^*_{\rm fus}$ for the ^{86}Kr + ^{130}Xe reaction is larger than that of the ^{124}Sn + ^{92}Zr reaction. Therefore, the fusion excitation function is lower for the former reaction than for the latter. The calculated angular momentum distribution of the fusion partial cross sections depend on both the intrinsic fusion and quasifission barriers. The volume under the surface $\sigma^{\ell}_{\rm fus}(E^*)$ for the ^{86}Kr + ^{130}Xe (II) reaction is smaller than that for the ^{124}Sn + ^{92}Zr (III) reaction (Fig. 6). This creates the necessary prerequisites to obtain larger cross sections of the evaporation residue for the latter (III) reaction in comparison with the former (II) one. The calculated results are in good agreement with the experimental data.

Therefore, the comparison and theoretical analysis of the experimental data on the evaporation residues in the ^{124}Sn + ^{92}Zr and ^{86}Kr + ^{130}Xe reactions leading to ^{216}Th* convince the importance of the shell structure in the fusion mechanism. This phenomenon is explained by the relationship between the intrinsic fusion ($B^*_{\rm fus}$) and quasifission ($B_{\rm qf}$) barriers for these reactions [see Fig. 2(c)].

(iii) The maximum of the experimental excitation functions of evaporation residues for the ^{48}Ca + ^{174}Yb (IV) reaction [5] is about two times higher than that for the ^{86}Kr + ^{136}Xe (V) reaction [3] [Fig. 8(c)], leading both reactions to the ^{222}Th* CN. This fact is explained by the large fusion cross section of the (IV) reaction [Fig. 8(b)], though at $E^* \geqslant 45$ MeV the fusion cross section of the ^{48}Ca + ^{174}Yb reaction reaches also more than one order of magnitude larger than the fusion cross section of the ^{86}Kr + ^{136}Xe reaction. Such large difference between the fusion cross sections is compensated by the different fission probability of nuclei formed in the above-mentioned reactions. The fission probability of the ^{222}Th* CN in the ^{48}Ca + ^{174}Yb (IV) reaction is higher than the fission probability of the ^{222}Th* CN obtained by the ^{86}Kr + ^{136}Xe (V) reaction because of the different dynamical effects (see Fig. 9) in the entrance channel. A higher average fission probability of the excited nuclei along the decay-chain of CN produces a lower evaporation residue formation, and this circumstance explains why the ratio between the evaporation residue cross sections is maximum 2 times for the reactions under consideration, though the ratio between the fusion cross sections reaches a more higher value (more than one order of magnitude).

(iv) Another interesting phenomenon that was observed in the comparison of the experimental data for reactions induced by the ^{86}Kr projectile on the ^{130}Xe and ^{136}Xe targets is that the ER cross section $\sigma_{ER}(E_{\rm c.m.})$ in ^{86}Kr + ^{130}Xe (II) was about 500 times smaller than that in ^{86}Kr + ^{136}Xe (V) [see Fig. 10(c)]. The experimental and theoretical excitation functions presented in Fig. 10(c) are the total evaporation residues after neutron emission only, along the deexcitation cascade of CN formed in the ^{86}Kr + ^{130}Xe and ^{86}Kr + ^{136}Xe reactions. These differences are caused by the dynamical and structural effects (see Fig. 11), which, in turn, are connected with the excess number of neutrons in the ^{136}Xe target in comparison with the ^{130}Xe one. Analyzing the mechanism of these reactions, we conclude that the fusion cross section of the reaction with the ^{136}Xe target is larger than the one of the reaction with the ^{130}Xe target because the intrinsic fusion barrier $B^*_{\rm fus}$ and $B^*_{\rm fus}/B_{\rm qf}$-ratio for the reaction with the ^{136}Xe target are smaller than the ones for the reaction with the ^{130}Xe target (see Tables I and II). In fact, both of these conditions stimulate a higher rate of the complete fusion in competition with the quasifission process for the reaction (V) in comparison with the reaction (II) [see Fig. 10(b)]. The excess number of neutrons lead to different fission probabilities along the various steps of the decay chain of the ^{222}Th* CN obtained by the ^{86}Kr + ^{136}Xe reaction, in comparison with the fission probability values obtained at the corresponding decay steps of ^{216}Th* obtained in the ^{86}Kr + ^{130}Xe reaction.

(v) To analyze the fusion-fission process, the fission excitation function presented in Ref. [2] for the ^{40}Ar + ^{176}Hf reaction were compared with the calculated fusion, quasifission, and fast-fission excitation functions. The calculated sum of fusion and fast-fission cross sections are in agreement with the data on the symmetric mass fragments [2] up to excitation energies E^* of about 65 MeV [Fig. 5(b)]. It means that the fragments of the fast-fission reaction contribute to the data of the mass symmetric fragments [2] at $E^* > 50$ MeV.

In summary, the difference between the measured cross sections of evaporation residues for different reactions in the entrance channel leading to the same compound nuclei can be explained by the difference in the excitation functions of fusion and the dependence of the fission probability of the excited compound nucleus (as well as intermediate excited nuclei) on their different angular momentum distributions. The decrease of the complete fusion cross sections is connected with the increase of the quasifission contributions. Competition between complete fusion and quasifission depends on the

dynamics of the entrance channel and the nuclear shell structure of colliding nuclei.

ACKNOWLEDGMENTS

Authors are grateful to Professors R. V. Jolos, J. Péter, V. V. Volkov, and W. Scheid and Drs. G. G. Adamian and N. V. Antonenko for the helpful discussions. This work was performed partially under the financial support of the RFBR (grant 04-02-17376) and INTAS (grant 03-01-6417). One of the authors (A.K.N.) thanks the Heisenberg-Landau Program for support while staying at the GSI, DFG, and RFBR (grant 01-02-16033) for financial support. Authors (A.I.M and A.K.N.) are grateful the Coordinating Council on Science and Technologies of the Uzbekistan's Government (grant F-2.1.8) and the Fond to support the Fundamental Research of the Academy of Science of Uzbekistan (No. 64-04) for partial support. A.K.N. expresses his gratitude for the warm hospitality during his stay at GSI, Giessen Justus-Liebig University (Germany), and University of Messina (Italy). R.N.S. and A.K.N. are also grateful to the Fondazione Bonino-Pulejo (FBP) of Messina for the support received in the collaboration with the Messina group.

[1] D. Vermeulen, H.-G. Clerc, C.-C. Sahm, K.-H. Schmidt, J. G. Keller, G. Münzenberg, and W. Reisdorf, Z. Phys. A **318**, 157 (1984).

[2] H.-G. Clerc, J. G. Keller, C.-C. Sahm, K.-H. Schmidt, H. Schulte, and D. Vermeulen, Nucl. Phys. **A419**, 571 (1984).

[3] R. N. Sagaidak, *et al*., in *Heavy Ion Physics: VI International School-Seminar, Dubna, Russia, 22–27 September 1997*, edited by Yu. Ts. Oganessian and R. Kalpakchieva (World Scientific, Singapore, 1998) 323; Yu. Ts. Oganessian, A. Yu. Lavrentev, A. G. Popeko, R. N. Sagaidak, A. V. Yeremin, S. Hofmann, F. P. Heßberger, V. Ninov, Ch. Stodel, *JINR FLNR Scientific Report 1995–1996: Heavy Ion Physics*, edited by B. I. Pustylnik (JINR, E7-97-206, Dubna, 1997), p. 62.

[4] C.-C. Sahm, H.-G. Clerc, K.-H. Schmidt, W. Reisdorf, P. Armbruster, F. P. Heßberger, J. G. Keller, G. Münzenberg, and D. Vermeulen, Nucl. Phys. **A441**, 316 (1985).

[5] R. N. Sagaidak, *et al*. *JINR FLNR Scientific Report 1997–1998: Heavy Ion Physics*, edited by A. G. Popeko, p. 60 (JINR, E7-2000-232, Dubna, 2000).

[6] G. G. Adamian, N. V. Antonenko, W. Scheid, and V. V. Volkov, Nucl. Phys. **A633**, 409c (1998).

[7] G. Giardina, S. Hofmann, A. I. Muminov, and A. K. Nasirov, Eur. Phys. J. A **8**, 205 (2000).

[8] E. A. Cherepanov, *International Conference on Nuclear Physics "Shells–50", Dubna, Russia, 1999*, edited by Yu. Ts. Oganessian and R. Kalpakchieva (World Scientific, Singapore, 2000), p. 266.

[9] A. K. Nasirov, A. Fukushima, Y. Toyoshima, Y. Aritomo, A. I. Muminov, Sh. Kalandarov, and R. K. Utamuratov, Nucl. Phys. **A759**, 342 (2005).

[10] N. V. Antonenko, E. A. Cherepanov, A. K. Nasirov, V. P. Permjakov, and V. V. Volkov, Phys. Lett. **B319**, 425 (1993); Phys. Rev. C **51**, 2635 (1995).

[11] E. A. Cherepanov, V. V. Volkov, N. A. Antonenko, and A. K. Nasirov, Nucl. Phys. **A459**, 145 (1996).

[12] G. Giardina, F. Hanappe, A. I. Muminov, A. K. Nasirov, and L. Stuttgé, Nucl. Phys. **A671**, 165 (2000).

[13] D. H. E. Gross, R. C. Nayak, and L. Satpathy, Z. Phys. A **299**, 63 (1981).

[14] P. Fröbrich, Phys. Rep. **116**, 337 (1984); Phys. Lett. **B215**, 36 (1988).

[15] R. Bock *et al*., Nucl. Phys. **A388**, 334 (1982).

[16] W. Q. Shen, J. Albinski, A. Gobbi, S. Gralla, K. D. Hildenbrand, N. Herrmann, J. Kuzminski, W. F. J. Müller, H. Stelzer, J. Tõke, B. B. Back, S. Bjornholm, and S. P. Sorensen, Phys. Rev. C **36**, 115 (1987).

[17] A. J. Pacheco, J. O. Fernández Niello, D. E. DiGregorio, M. di Tada, J. E. Testoni, Y. Chan, E. Chávez, S. Gazes, E. Plagnol, and R. G. Stokstad, Phys. Rev. C **45**, 2861 (1992).

[18] B. B. Back, P. B. Fernandez, B. G. Glagola, D. Henderson, S. Kaufman, J. G. Keller, S. J. Sanders, F. Videbaek, T. F. Wang, and B. D. Wilkins, Phys. Rev. C **53**, 1734 (1996).

[19] M. G. Itkis *et al*., Nuovo Cimento Soc. Ital. Fis. A **111**, 783 (1998).

[20] M. G. Itkis *et al*., In *Proceedings of the Symposium on Nuclear Cluster, Rauischolzhausen, Germany*, edited by R. V. Jolos and W. Scheid, (EP Systema, Debrecen, 2003), 315 (2003); M. G. Itkis *et al*., Acta Phys. Hung. A **19**, 9 (2004).

[21] A. J. Sierk, Phys. Rev. C **33**, 2039 (1986).

[22] G. Fazio, *et al*., Eur. Phys. J. A **19**, 89 (2004).

[23] G. Fazio, *et al*., J. Phys. Soc. Jpn. **72**, 2509 (2003).

[24] Y. Aritomo and M. Ohta, Nucl. Phys. **A744**, 3 (2004).

[25] M. Trotta *et al*., Nucl. Phys. **A734**, 245 (2004).

[26] A. A. Sonzogni, R. Vandenbosch, A. L. Caraley, and J. P. Lestone, Phys. Rev. C **58**, 1873(R) (1998).

[27] D. J. Hinde, M. Dasgupta, J. R. Leigh, J. P. Lestone, J. C. Mein, C. R. Morton, J. O. Newton, and H. Timmers , Phys. Rev. Lett. **74**, 1295 (1995).

[28] D. J. Hinde, M. Dasgupta, J. R. Leigh, J. C. Mein, C. R. Morton, J. O. Newton, and H. Timmers , Phys. Rev. C **53**, 1290 (1996).

[29] J. F. Liang *et al*., Nucl. Phys. **A746**, 103 (2004).

[30] A. C. Berriman, D. J. Hinde, M. Dasgupta, C. R. Morton, R. D. Butt, and J. O. Newton, Nature (London) **413**, 144 (2001).

[31] D. J. Hinde, M. Dasgupta, and A. Mukherjee, Phys. Rev. Lett. **89**, 282701 (2002).

[32] G. Fazio, G. Giardina, A. Lamberto, A. I. Muminov, A. K. Nasirov, F. Hanappe, and L. Stuttgé, Eur. Phys. J. A **22**, 75 (2004).

[33] M. Dasgupta and D. J. Hinde, Nucl. Phys. **A734**, 148 (2004).

[34] G. G. Adamian, N. V. Antonenko, and W. Scheid, Phys. Rev. C **68**, 034601 (2003).

[35] A. K. Nasirov, G. Giardina, A. I. Muminov, W. Scheid, and U. T. Yakhshiev, in *Proceeding of the Symposium on Nuclear Cluster, Rauischolzhausen, Germany*, edited by R. V. Jolos and W. Scheid, 2003 (EP Systema, Debrecen, 2002), p. 415; Acta Phys. Hung. A **19**, 109 (2004).

[36] A. D'Arrigo, G. Giardina, M. Herman, A. V. Ignatyuk, and A. Taccone, J. Phys. G **20**, 365 (1994).

[37] A. D'Arrigo, G. Giardina, M. Herman, and A. Taccone, Phys. Rev. C **46**, 1437 (1992).

[38] R. N. Sagaidak, *et al*., J. Phys. G **24**, 611 (1998).
[39] G. Fazio *et al*., J. Phys. Soc. Jpn. **74**, 307 (2005).
[40] G. Fazio, G. Giardina, G. Mandaglio, F. Hanappe, A. I. Muminov, A. K. Nasirov, W. Scheid, and L. Stuttgé, Mod. Phys. Lett. A **20**, 391 (2005).
[41] G. G. Adamian, R. V. Jolos, A. K. Nasirov, and A. I. Muminov, Phys. Rev. C **56**, 373 (1997).
[42] D. Ackermann *et al*., Nucl. Phys. **A630**, 442c (1998).
[43] G. Audi and A. H. Wapstra, Nucl. Phys. **A595**, 409 (1995); A. H. Wapstra and G. Audi, Nucl. Phys. **A432**, 1 (1985).
[44] R. V. Jolos, A. I. Muminov, and A. K. Nasirov, Sov. J. Nucl. Phys. **44**, 228 (1986).
[45] P. Möller and J. R. Nix, At. Data Nucl. Data Tables **39**, 213 (1988).
[46] S. Raman, C. H. Malarkey, W. T. Milner, C. W. Nestor, Jr., and P. H. Stelson, At. Data Nucl. Data Tables **36**, 1 (1987).
[47] R. H. Spear, At. Data Nucl. Data Tables **42**, No. 1, 55 (1989).
[48] G. G. Adamian, N. V. Antonenko, and W. Scheid, Nucl. Phys. **A618**, 176 (1997).
[49] G. G. Adamian, N. V. Antonenko, W. Scheid, and V. V. Volkov, Nucl. Phys. **A627**, 361 (1997).
[50] G. G. Adamian, N. V. Antonenko, and W. Scheid, Phys. Rev. C **69**, 014607 (2004).
[51] S. Hofmann, Rep. Prog. Phys. **61**, 639 (1998); S. Hofmann, Z. Phys. A **358**, 125 (1997).
[52] J. P. Blocki, H. Feldmeier, and W. J. Swiatecki, Nucl. Phys. **A459**, 145 (1986).